On the Role of a Nonlinear Stress-Strain Relation in Brain Trauma

Igor Szczyrba
School of Mathematical Sciences
University of Northern Colorado
Greeley, CO 80639, U.S.A.

Martin Burtscher
Center for Grid and Distributed Computing
The University of Texas at Austin
Austin, TX 78712, U.S.A.

Rafal Szczyrba
Funiosoft, LLC
Silverthorne, CO 80498, U.S.A.

Abstract *We investigate how a nonlinear stress-strain relation (that leads to a stiffening of the brain matter under strain) influences the brain dynamics in traumatic situations. We numerically simulate rapid rotational accelerations and decelerations of a human head using our generalization of the viscoelastic Kelvin-Voigt brain injury model that includes an experimentally established dependency of stress on strain. The rotational loads are expressed in terms of the Brain Injury Criterion, which we developed to extend the translational Head Injury Criterion to arbitrary head motions. Under traumatic loads corresponding to $HIC_{15} = 700$, our model predicts that the brain stiffening reduces the maximal strain near the skull by up to 70%, but leads to a distribution of relatively high strain values throughout the brain. We show how the brain's complex geometry enhances the random spatial distribution of high strain values.*

Keywords: brain injury modeling, nonlinear stress-strain relation

1 Introduction

The human brain is a viscoelastic medium. It is widely accepted that Traumatic Brain Injuries (TBI) not accompanied by a fractured skull are caused by the shear waves created in the brain during traumatic situations. One of the most commonly used approaches in brain injury modeling treats the brain as a viscoelastic solid and describes the propagation of shear waves within the brain by means of the linear Kelvin-Voigt (K-V) partial differential equations (PDEs):

$$\frac{\partial \mathbf{v}}{\partial t} = c^2 \triangle \mathbf{u} + \nu \triangle \mathbf{v}, \quad \frac{\partial \mathbf{u}}{\partial t} = \mathbf{v}, \quad \nabla \cdot \mathbf{u} = 0, \tag{1}$$

where $\mathbf{v}(\mathbf{x}, t)$ with $\mathbf{x}=(x_1, x_2, x_3)$ is the time-dependent velocity vector field, $\mathbf{u}(\mathbf{x}, t)$ denotes the corresponding displacement vector field, $c \equiv \sqrt{G/\delta}$ is the *constant* phase velocity of the shear waves (with G and δ being the shear modulus and the density of the brain matter, respectively), and ν denotes the kinematic viscosity.

Analytic solutions of (1), known only for impulsive central rotations of a head with an idealized shape (i.e., circular or spherical symmetry), have been successfully used in the past for modeling brain hematomas and Diffuse Axonal Injuries (DAI), cf. [1, 2]. More recent experiments indicate, however, that the brain matter stiffens under strain, meaning that the shear wave velocity changes when the brain tissue is strained. Experimental data imply that the stress-strain relation can be approximated by an exponential function but various experimental settings provide a wide range for the exponential coefficient [3, 4].

Thus, we generalize system (1) by replacing c^2 with $c^2(\mathbf{x}, t) = c^2 e^{pN(\mathbf{x},t)}$, where c is the 'basic' shear wave velocity (i.e., in the absence of strain), p is a coefficient within the range implied by experiments, i.e., $0.4 \le p \le 2.5$, and $N(\mathbf{x}, t)$ is the operator norm of the strain (Jacobi) matrix of the brain matter relative (with respect to the skull) displacement $\mathbf{U}(\mathbf{x}, t)$, i.e.,

$$N(\mathbf{x}, t) \equiv \sup_{\|\mathbf{y}\|=1} \| \frac{\partial \mathbf{U}}{\partial \mathbf{x}}(\mathbf{x}, t) \cdot \mathbf{y} \|, \quad \mathbf{y} = (y_1, y_2, y_3). \tag{2}$$

These nonlinear PDEs are hard to solve and (to our knowledge) no prior solutions have been reported.

2 Solution Method and Simulation Setup

Our linear analysis of (1) implies that the shortest shear waves that can propagate in human brain matter are *circa* 10^{-2}m in length [5]. Consequently, shear wave modeling requires the distance between computational nodes not to exceed $\Delta x{=}2{\cdot}10^{-3}$m. To maintain this resolution while numerically solving system (1) with $c^2(\mathbf{x},t)$, we use the Finite Difference Method[1]. The solutions presented in this paper are obtained using the grid size $\Delta x{=}10^{-3}$m, and they are numerically stable only if the time step $\Delta t \leq 10^{-5}$s. The stability of the solutions is constantly monitored by means of the standard Courant and Lipschitz parameters.

To properly study the impact of a nonlinear stress-strain relation on the brain dynamics, we have to exclude the influence of the differences in the physical properties between the gray and the white matter on the propagation of shear waves as well as the cushioning role of the layers between the skull and the brain. Thus, we assume the brain tissue to be uniform and firmly attached to the skull (*dura* matter), with the basic shear wave velocity $c{=}1$m/s, viscosity $\nu{=}0.01\text{m}^2/\text{s}$, and density $\delta{=}1.06{\times}10^3\,\text{kg/m}^3$.

First, we simulate rotational accelerations and decelerations of an ideal head with circular symmetry about a fixed axis positioned in its center. This allows us to limit the solutions to a 2D circular cross-section of the brain and to verify the results with the existing analytic solution. This enables us also to separate the role of the brain's complex geometry from the role of a nonlinear stress-strain relation in the TBI creation, cf. [9]. Next, we investigate the consequences of minor violations of the cross-section's circular symmetry.

Finally, we simulate the same rotations of a realistic human head about fixed vertical and horizontal axes positioned at the brain's center of mass. The contours of the 2D brain cross-sections, perpendicular to the axes, are derived using cubic spline interpolations of digitized medical data. The choice of the vertical axis enables us to consider horizontal brain cross-sections that (near the top of the head) constitute disconnected domains separated by the *falx cerebri*. Conversely, the positioning of the horizontal axis through the ears allows us to consider simply-connected sagittal cross-sections that do not include any part of the *falx cerebri*.

We use the strain-dependent shear wave velocity $c^2(\mathbf{x},t){=}c^2e^{pN(\mathbf{x},t)}$ with $p=0.4$, 1.1, 1.8 and 2.5, and assume that the stiffening of the brain tissue is limited, i.e., $c^2(\mathbf{x},t)\leq 50$. We simulate two types of loads, each lasting for $T{=}0.015$s. The first load $\mathcal{D}$ decelerates the head from a constant clockwise rotation to zero with a triangularly shaped tangential deceleration, Fig. 1a and 1b. The second load $\mathcal{A}$ accelerates the head clockwise from zero and then decelerates it until the head rests, Fig. 1c and 1d. Both load types have the same Brain Injury Criterion value $BIC_{15}{=}700$. This means that during time T, the same maximal average power's absolute value is exchanged between the skull and the brain per unit mass through a brain region near the 2D cross-section as through any brain region during a head translation with the Head Injury Criterion value $HIC_{15}{=}700$, cf. [7, 10] for details. Head motions corresponding to $HIC_{15}{=}700$ are believed to cause very serious brain injuries [11, 12].

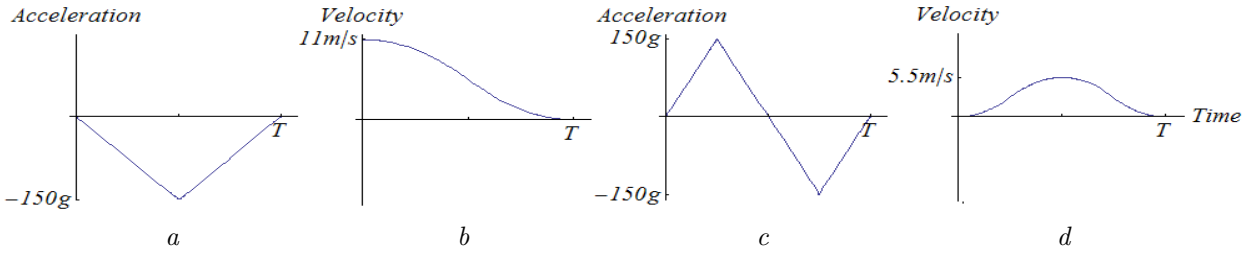

Figure 1:
Tangential acceleration and velocity of the rotated head corresponding to $BIC_{1000T}{=}700$ with $T{=}0.015$s; Decelerated motion $\mathcal{D}$ — panels *a* and *b*; Accelerated/decelerated motion $\mathcal{A}$ — panels *c* and *d*.

To illustrate the impact of distinct nonlinear stress-strain relations on TBI creation, we depict (for certain critical times t) the strain norm $N(\mathbf{x},t)$ defined in (2) as well as the absolute values of the brain matter's relative (with respect to the skull) displacement $\mathbf{U}(\mathbf{x},t)$ and velocity $\mathbf{V}(\mathbf{x},t)$. We also present snapshots of Curved Vector Field plot animations that visualize the temporal evolution of the velocity fields $\mathbf{V}(\mathbf{x},t)$ in various 2D brain cross-sections. The animations are available at http://www.funiosoft.com/brain/.

[1]Our previous simulations, cf. [6, 7], based on system (1) and our fluid extension of this system indicate that short shear waves seem to play a crucial role in the creation of DAI (caused predominately by rapid head rotations, cf. [8]). To our knowledge, TBI models utilizing the Finite Element Method have not yet been designed to model very short shear waves.

3 Numerical Results

An ideal head with circular symmetry under the $\mathcal{D}$ load

Analytic solutions of (1) show that an instant deceleration of an ideal head from a constant rotation about the head's center creates shear waves of length equal to the head's diameter [1]. Our simulation of a continuous head deceleration $\mathcal{D}$ with $p=0$ leads to a similar result. In this case, the global maxima of the relative displacement's absolute value and of the corresponding strain norm are assumed at $t\approx 0.025$s, giving rise to $|\mathbf{U}|_{\max}=0.1$m, Fig. 2a, and $N_{\max}=5.3$, Fig. 2b, respectively[2]. The vertical cross-section of Fig. 2a along a radius shows the deformation of the brain matter that takes place in the circular cross-section. Indeed, during (and for some time after) the deceleration, the brain matter deforms with respect to the skull in the clockwise direction of the rotation trying to maintain the original rotational velocity.

For $t\geq 0.025$s, the brain matter begins to rotate in the counter-clockwise direction about the center and the oscillations continue back and forth. Before the wave is dampened, it propagates towards the center maintaining its magnitude for 0.06s but changing essentially its shape, cf. Fig. 2c. Fig. 2d shows that at $t=0.06$s, the norm values are halved near the skull to 2.6 but doubled from 1.9 to 3.8 near the center. $|\mathbf{V}|_{\max}=6.4$m/s (assumed near the skull at $t=0.013$s) drops at $t=0.06$s by almost 50% to 3.3m/s, and the graphs of $|\mathbf{V}|$ (not shown here) closely resemble Figs. 2a and 2c.

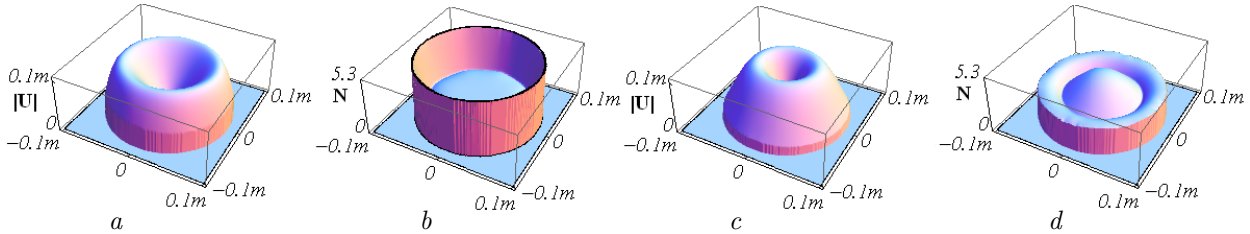

Figure 2:
The values of $|\mathbf{U}|$ and N in the circular cross-section assumed under the $\mathcal{D}$ load with $p=0$ at $t=0.025$s — panels a and b, and at $t=0.06$s — panels c and d.

Simulations of an ideal head under the $\mathcal{D}$ load with $0<p\leq 2.5$ result in a 60% reduction of $|\mathbf{U}|_{\max}$ and 68% of $N_{\max}$, while $|\mathbf{V}|_{\max}$ is reduced only by 19%. Thus, $|\mathbf{U}|_{\max}$ drops linearly from 0.1m to 0.04m, $N_{\max}$ exponentially from 5.3 to 1.7, and $|\mathbf{V}|_{\max}$ from 6.4m/s to 5.2m/s with the biggest reduction for large p. All maximal values are assumed earlier with larger p, e.g., for $p=2.5$, at $t=0.01$s. Moreover, the brain matter oscillations become more frequent and the shear waves propagate faster towards the center.

A head with 'almost' circular symmetry under the $\mathcal{D}$ load

Solutions of (1) with a strain-dependent wave velocity $c^2(\mathbf{x},t)$ are chaotic, i.e., they are very sensitive to the boundary conditions *ergo* the brain's geometry. As is shown in Fig. 3, a very minor violation of the circular symmetry leads to quite large fluctuations of the $|\mathbf{U}|$ and N values. Specifically, Figs. 3a and 3b depict $|\mathbf{U}|$ and N at $t=0.04$s after the $\mathcal{D}$ deceleration with $p=1.1$, whereas Figs. 3c and 3d show fluctuations of the norm N when $p=1.8$ and $p=2.5$, respectively. The functions are shown from 'below' to better present the features of the fluctuations. In all these cases, the fluctuations of $|\mathbf{V}|$ are negligible.

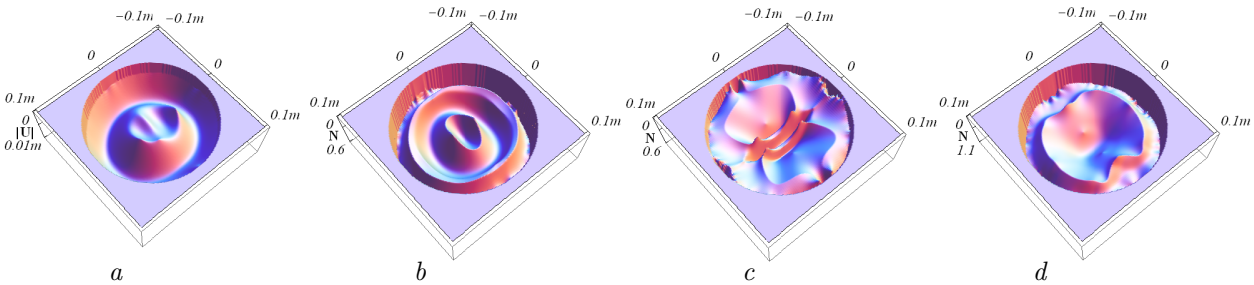

Figure 3:
The values of $|\mathbf{U}|$ and N in the 'almost' circular cross-section assumed under the $\mathcal{D}$ load with $p=1.1$ at $t=0.04$s — panels a and b, with $p=1.8$ at $t=0.06$s — panel c, and with $p=2.5$ at $t=0.035$s — panel d.

[2]These values are high since we do not include the strain-mitigating layer between the skull and the brain and use the basic wave velocity $c=1$m/s, which (being at the lower end of the experimental data) allows the creation of very short waves, cf. [5].

As will be shown below, the observed fluctuations of the norm values become larger when the complicated realistic geometry of the brain is introduced. Thus, the nonlinearity of the stress-strain relation could at least partially[3] explain why DAI are scattered through the entire brain matter in a pointwise manner, i.e., some neurons are injured whereas neighboring neurons are not [13, 14].

An ideal and 'almost' ideal head under the $\mathcal{A}$ load

Simulations with the $\mathcal{A}$ load lead to smaller values of $|\mathbf{U}|_{\max}$ and $N_{\max}$ as well as a smaller value reductions with larger p. $|\mathbf{U}|_{\max}$ diminishes only by 15% from 0.026m when $p=0$ to 0.022m when $p=2.5$, whereas $N_{\max}$, which in this case is assumed at $t\approx 0.009$s, drops by 40% from 2.0 to 1.2. Surprisingly, $|\mathbf{V}|_{\max}$ rises by 23% from 3.9m/s to 4.8m/s when p is increased even though, in this case, the frequency of the brain oscillations remains unchanged when p increases.

Nevertheless, these simulations reveal a very important consequence of the nonlinear stress-strain relation. Namely, after the $\mathcal{A}$ load is applied to the circular or 'almost' circular cross-section, the damping of the shear waves is accompanied by a shortening of their length by a factor of two. That creates relatively high norm values in the middle of the cross-section (even with the ideal circular symmetry). An increase of p speeds up this process. Consequently, for $p>0$, the norm values in the middle are larger than when $p=0$. As in the case of the $\mathcal{D}$ load, a minor violation of circular symmetry leads to essential changes in the spatial distribution of large norm values but does not influence the conic shapes of $|\mathbf{V}|$ (resembling Fig. 4a).

Figs. 4 and 5 depict the values of $|\mathbf{U}|$ and N assumed in the 'almost' circular cross-section under the $\mathcal{A}$ load with $p=0$ and $p=2.5$, respectively. Note that in Figs. 4c and 5a, the wave length equals to the radius (and not to the diameter) of a given circular cross-section—and the vertical cross-sections of $|\mathbf{U}|$ along radii represent the *absolute* values of the brain matter deformations that take place in this cross-section. Fig. 5b shows that in comparison to the case where $p=0$ (Fig. 4d), the stiffening of the brain matter creates high strain values in the entire cross-section much earlier, i.e., at $t=0.02$s *versus* $t=0.045$s. Consequently, the strain values are much higher in the interior of the cross-section (approximately 50% higher when $p=2.5$). Similarly to the case of the $\mathcal{D}$ load, a minor violation of circular symmetry causes fluctuations of the norm values for $p>0$ when the wave length coincides with the diameter of the circular cross-sections (compare Figs. 4b and 5d) but does not modify, in an essential way, the distribution of $|\mathbf{V}|$.

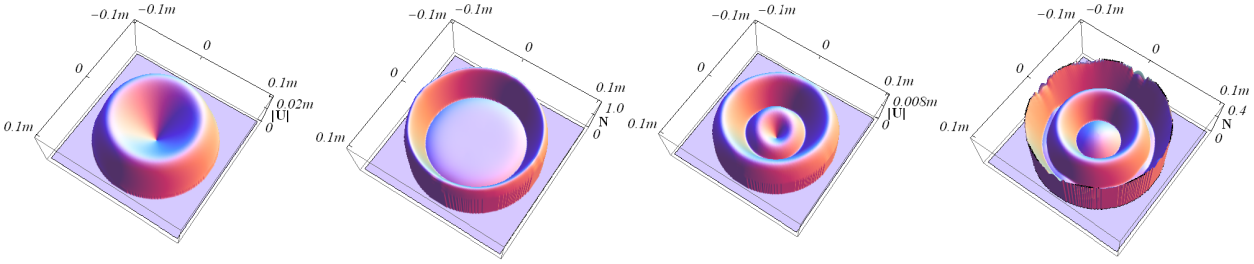

Figure 4:
The values of $|\mathbf{U}|$ and N in the 'almost' circular cross-section assumed under the $\mathcal{A}$ load with $p=0$ at $t=0.02$s — panels *a* and *b*, and at $t=0.045$s — panels *c* and *d*.

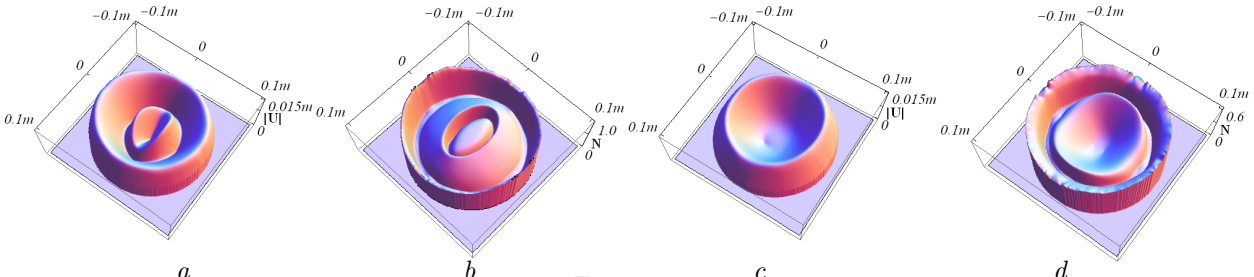

Figure 5:
The values of $|\mathbf{U}|$ and N in the 'almost' circular cross-section assumed under the $\mathcal{A}$ load with $p=2.5$ at $t=0.02$s — panels *a* and *b*, and at $t=0.045$s — panels *c* and *d*.

[3]The fluid character of the brain tissue (which consists of *circa* 80% water) may be another reason why DAI are scattered in a pointwise manner, cf. [6, 7] where results of simulations based on our fluid nonlinear generalization of the K-V model (with a linear stress-strain relation) are presented.

A realistic head under the $\mathcal{D}$ and $\mathcal{A}$ loads

A realistic brain geometry dramatically changes the shape of the solutions. First, for all p values, the norm values vary extensively near the skull—assuming local maxima where the curvature of the cross-section's boundary is large. Second, high strain values 'spread' quickly into the brain's interior forming quite erratic patterns. Third, the distribution of $|\mathbf{V}|$ becomes erratic as well. The fluctuations of the norm, displacement and velocity values as well as the shortening of the wave lengths are enhanced and sped up as p increases.

In the case of a sagittal brain cross-section and $\mathcal{D}$ load with $p=0$, the maximal values of $|\mathbf{U}|_{\max}$, $N_{\max}$, and $|\mathbf{V}|_{\max}$ as well as the times at which they are assumed are very similar to those obtained for the circular cross-section. However, contrary to the circular case, high values of these functions appear now in the cross-section's interior as well, cf. Fig. 6 where, for the consistency of presentation, the graph of $|\mathbf{V}|$ is shown for $t=0.025$s and not for $t=0.01$s when $|\mathbf{V}|_{\max}=5.0$m/s is assumed. This shows that the brain's geometry plays a crucial role in the localization of TBI. An increase of p under the $\mathcal{D}$ load diminishes the values of $N_{\max}$ by 70%, $|\mathbf{U}|_{\max}$ remains almost the same, while $|\mathbf{V}|_{\max}$ increases. Fig. 7 illustrates that for $p=2.5$, all three functions exhibit at $t=T=0.15$s patterns that are characteristic for the propagation of short shear waves.

Simulations of the sagittal cross-section under the $\mathcal{A}$ load confirm that the stiffening of the brain matter under strain induces shorter shear waves that create high strain values in the brain interior. The complicated brain geometry enhances the random distribution of these high strain values throughout the entire brain. Fig. 8 illustrates these results by depicting the values of $|\mathbf{U}|$, N, and $|\mathbf{V}|$ at $t=0.03$s obtained with $p=2.5$.

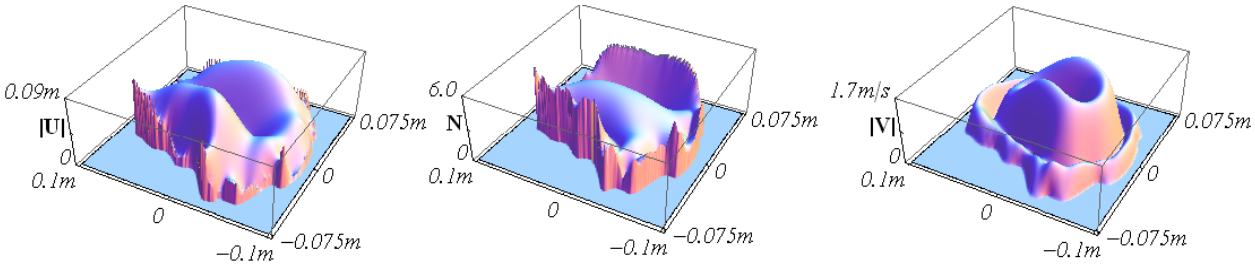

Figure 6:
The values of $|\mathbf{U}|$, N, and $|\mathbf{V}|$, respectively, in a sagittal cross-section assumed under the $\mathcal{D}$ load with $p=0$ at $t=0.025$s.

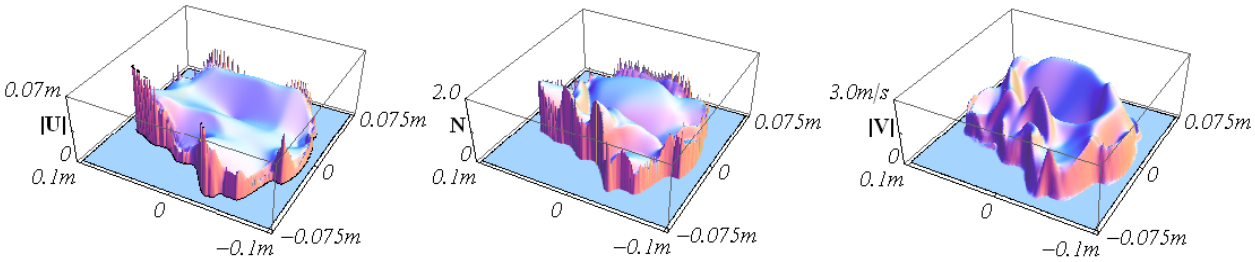

Figure 7:
The values of $|\mathbf{U}|$, N, and $|\mathbf{V}|$, respectively, in a sagittal cross-section assumed under the $\mathcal{D}$ load with $p=2.5$ at $t=0.015$s.

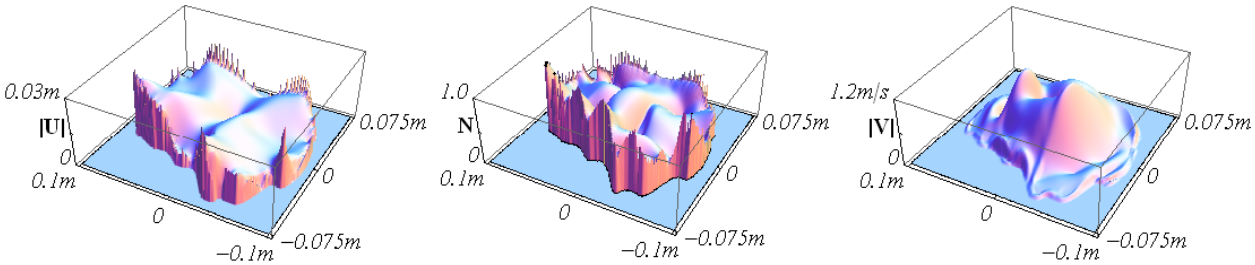

Figure 8:
The values of $|\mathbf{U}|$, N, and $|\mathbf{V}|$, respectively, in a sagittal cross-section assumed under the $\mathcal{A}$ load with $p=2.5$ at $t=0.03$s.

Since $|\mathbf{U}|=0$ at the *dura matter*, the presence of the *falx cerebri* in the horizontal cross-section limits the length of the waves deforming the brain in the direction parallel to the *falx cerebri* as well as the range of the brain deformations in the perpendicular direction. This impact of the *falx cerebri* is illustrated in Figs. 9 and 10, where the values of $|\mathbf{U}|$ are half of those in the sagittal cross-section. Also, contrary to the result in the sagittal cross-section, the values of $|\mathbf{V}|$ more rapidly drop in time for large p, compare Figs. 6 and 7.

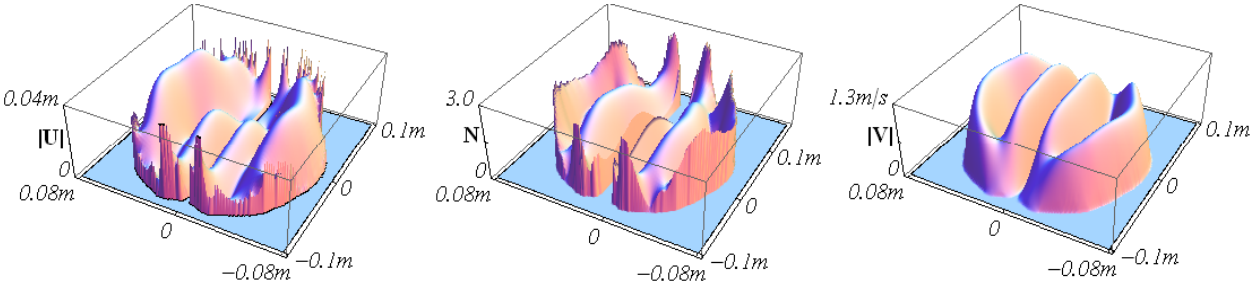

Figure 9:
The values of $|\mathbf{U}|$, N, and $|\mathbf{V}|$, respectively, in a horizontal cross-section assumed under the $\mathcal{D}$ load with $p=0$ at $t=0.03$s.

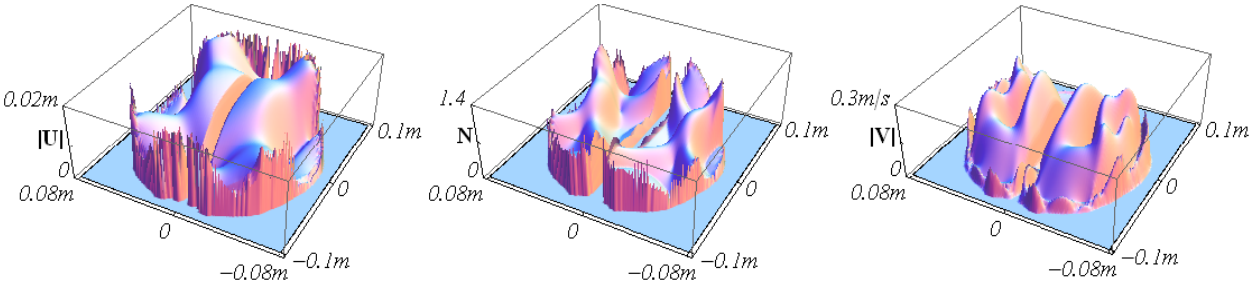

Figure 10:
The values of $|\mathbf{U}|$, N, and $|\mathbf{V}|$, respectively, in a horizontal cross-section assumed under the $\mathcal{D}$ load with $p=2.5$ at $t=0.03$s.

Fig. 11 shows how the stiffening of the brain matter modifies the character of the brain matter oscillations. The dark to light shading of the curved velocity vectors indicates the direction of the brain matter motion relative to the skull. The velocity fields $\mathbf{V}(\mathbf{x},t)$ are shown at $t=0.01$s in the sagittal and horizontal cross-sections under the $\mathcal{D}$ load. For $p=0$, the brain matter oscillates in a circular manner, Figs. 11a and 11c, whereas for $p=2.5$, multi-vortex oscillatory patterns arise, Figs. 11b and 11d. Similar patterns appeared during simulations based on our fluid nonlinear generalization of system (1), in which the temporal partial derivative in (1) is replaced by the (nonlinear) material derivative, cf. [6, 7]. Thus, to fully explain the random spatial distribution of DAI, we are developing a dually nonlinear generalization of system (1).

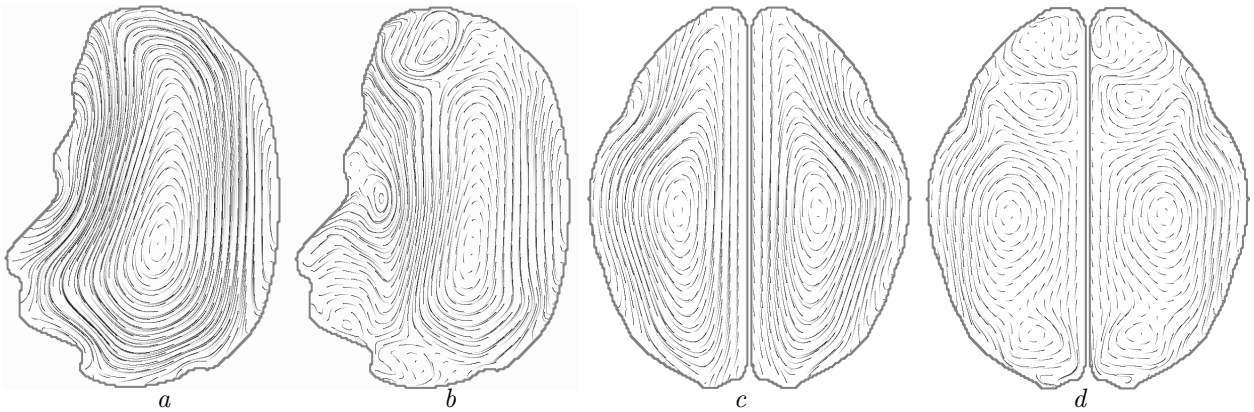

Figure 11:
The velocity fields $\mathbf{V}(\mathbf{x},t)$ in sagittal and horizontal cross-sections at $t=0.01$s under the $\mathcal{D}$ load with $p=0$ — panels a and c, and $p=2.5$ — panels b and d.

4 Conclusions

Our numerical simulations based on the K-V system (1) with a nonlinear stress-strain relation show that the stiffening of the brain matter under strain diminishes the maximum strain values overall, especially near the skull. However, it simultaneously leads to relatively higher strain values (in comparison to the values obtained with the linear K-V PDEs) in the brain interior due to the shortening of the shear wave lengths.

The complicated geometry of the human brain, in particular the existence of the *falx cerebri*, enhances this effect. Consequently, the distribution of high strain values throughout the brain becomes random (which matches DAI observations).

5 Acknowledgment

The simulations for this study were partially performed on a multiprocessor workstation funded by the Research Enrichment and Development Initiative at the University of Northern Colorado. Martin Burtscher has been supported by NSF grants CNS-0724966 and CNS-0719966 as well as by grants from IBM and Intel.

References

[1] C. Ljung. A Model for Brain Deformation due to Rotation of the Skull. *J. Biomech.*, 8:263-274, 1975.

[2] S. S. Margulies and L. Thibault. A Proposed Tolerance Criterion for Diffuse Axonal Injury in Man. *J. Biomech.*, 25:917-923, 1992.

[3] B. R. Donnelly and J. Medige. Shear Properties of Human Brain Tissue. *J. Biomech. Engineering* 119:423-432, 1997.

[4] E. G. Takhounts, J. R. Crandall and K. Darvish. On The Importance of Nonlinearity of Brain Tissue Under Large Deformations. *Stapp Car Crash J.,* 47:79-92, 2003.

[5] C. S. Cotter, P. K. Smolarkiewicz and I. N. Szczyrba. A Viscoelastic Fluid Model for Brain Injuries. *Int. J. for Numerical Methods in Fluids*, 40:303-311, 2002.

[6] M. Burtscher and I. Szczyrba. Computational Simulation and Visualization of Traumatic Brain Injuries. *Proc. MSV'06*, 101-107, CSREA Press 2006.

[7] I. Szczyrba, M. Burtscher and R. Szczyrba. Computational Modeling of Brain Dynamics during Repetitive Head Motions. *Proc. MSV'07*, 143-149, CSREA Press 2007.

[8] J. Meythaler *et al.* Amantadine to Improve Neurorecovery in Traumatic Brain Injury-associated Diffuse Axonal Injury. *J. of Head Trauma and Rehabilitation*, 17(4):303-313, 2002.

[9] M. Burtscher and I. Szczyrba. On the Role of the Brain's Geometry in Closed Head Injuries, *Proc. of the ASME 2005 Bioengin. Conf.*, SBC 2005 - b0010704.

[10] I. Szczyrba, M. Burtscher and R. Szczyrba. A Proposed New Brain Injury Tolerance Criterion based on the Exchange of Energy Between the Skull and the Brain. *Proc. of the ASME 2007 Summer Bioeng. Conf.*, SBC 2007 - 171967.

[11] M. Kleinberger *et al.* Development of Improved Injury Criteria for the Assessment of Advanced Automotive Restraint Systems. NHTSA 1998, http://www-nrd.nhtsa.dot.gov/pdf/nrd-11/airbags/criteria.pdf

[12] R. Eppinger *et al.* Development of Improved Injury Criteria for the Assessment of Advanced Automotive Restraint Systems-II. NHTSA 2000, http://www-nrd.nhtsa.dot.gov/pdf/nrd-11/airbags/finalrule_all.pdf

[13] W. Maxwell, J. Povlishock and D. Graham. A Mechanistic Analysis of Nondisruptive Axonal Injury: A Review. *J. of Neurotrauma*, 14:419-440, 1997.

[14] P. Leclerco *et al.* Axonal Injury is Accentuated in the Caudal Corpus Callosum of Head-Injured Patients *J. of Neurotrauma*, 18:1-10, 2001.